

## **Analysis of Boundary Layer Meteorological Data Collected at the White Sands Missile Range**

Sean O'Brien, David Tofsted, Jimmy Yarbrough, D. Scott Elliott, and David Quintis

U.S. Army Research Laboratory  
Computational and Information Sciences Directorate  
White Sands Missile Range, NM 88002  
[sobrien@arl.army.mil](mailto:sobrien@arl.army.mil)  
Ph: (505) 678-1570  
FAX: (505) 678-3385

### **Abstract**

During the late spring and summer of 2007, a series of near-surface measurements of winds, temperature, radiative fluxes and absolute humidity were collected at an observing site located on the White Sands Missile Range (WSMR). Our primary motivation for collecting these measurements is to refine the accuracy of outer and inner scale effects models for optical, thermal, and absolute humidity turbulence for the desert boundary layer. The sampling rate for the wind and humidity measurements was selected to be 20 Hz for both for consistency and for fluctuation spectra and turbulent flux calculation purposes. Simultaneous supporting measurements of temperature, upward and downward visible fluxes, and upward and downward long wave infrared (LWIR) fluxes were collected at a 1 Hz sampling rate. We describe the test methodology, analysis techniques and results, and applications for our test results.

### **1. Introduction**

The Battlefield Environment Division of the Army Research Laboratory (ARL) has extensively studied boundary layer meteorology to further our knowledge of atmospheric influences on developing battlefield sensing technologies (see, for example, Tofsted, et al., 2006). One of these emerging technologies is imaging sensors operating in the terahertz band of the electromagnetic spectrum. This band features radiation wavelengths of approximately 0.5 mm (500 microns) or less. There is significant atmospheric water vapor absorption in this waveband which, even in "window" regions of the spectrum, is typically greater than 0.1 dB/m. The resulting limits on the effective ranges of terahertz imaging equipment therefore greatly depend upon the state of the atmosphere, since the amount of water vapor present is a strong function of ambient temperature and airmass history.

There is considerable uncertainty regarding the overall degree of variation possible in the path integrated moisture profile, which depends on turbulent fluctuations in the atmospheric absolute humidity field. Although some knowledge of these fluctuations is available, based on studies of "conservative passive additive" scalar fluctuation effects featured in dynamic similarity theory, humidity influences must be treated somewhat differently from temperature influences. In particular, temperature fluctuations are

derived from heat transfers at the surface, whereas humidity sources can arise from spatially localized vegetative or surface water features, and can have a more complex emission rate phenomenology. This raises several questions regarding the structure of humidity fluctuations. For instance, are there feasible methods (such as air mass trajectory analysis) to determine source regions of an observed water vapor field? What are the important details of the mechanism that creates humidity fluctuations from standing pools of water, grass, shrubbery, and trees as they are ventilated by ambient winds? Do these sources somehow exhibit different characteristic signatures? What are the influences of anthropogenic effects such as buildings and landscaping on water source emissions?

Because of a traditionally agricultural orientation, most water vapor studies to date (but not all – see, for example, Cooper, et al., 2004) have been primarily concerned with evaporation of water from roughly uniform crop surfaces. Our interest is primarily in urban and short-range settings that may feature individualized (non-uniform) water sources. We are interested in both horizontal and vertical fluctuations. We are also interested in the spatial spectral nature of these fluctuations since fluctuations at different size scales will have different influences on the propagation problem. For instance, large fluctuations at small scales may be significant, leading to image degradation, whereas large scale fluctuations may not be significant at all, since they merely contribute to the overall extinction along a path.

With these questions in mind, we designed a series of boundary layer measurements for wind, temperature, surface radiation flux, and water vapor fluctuations that were conducted over a continuous span of time at a local site in desert terrain. The measurements for this Boundary Layer Terahertz (BLT) test were carried out in phases, described below, where sensor siting geometry was varied. The information provided by these inquiries will be very helpful in improving the accuracy of terahertz image propagation and sensor performance models (O'Brien and Tofsted, 2006), particularly in situations where the sensor system will have a large field of view or field of regard. Our studies will also provide insight into the structure and dynamic behavior of the local nocturnal stable boundary layer (SBL).

#### 1) Geographical description of the test site

A White Sands Missile Range, New Mexico (WSMR) test site was chosen on the basis of convenience and security for the ARL staff who conducted and maintained the experiment. The measurement instruments were sited next to an equipment compound, outside of the fence perimeter. The terrain at the test site is nearly flat, but slopes slightly toward the northeast. Spurs of the Organ Mountains are nearby, to the west and southwest of the test site. Figure 1 is a satellite image of the terrain near the test site extracted from the Internet, with some contrast enhancement applied to reduce atmospheric haze. The image also shows the approximate location of a horizontal measurement array of sensors used during the measurement series. The area is sparsely vegetated with plants that are typical of the Chihuahuan desert environment: mesquite, creosote bush, and various species of yucca. There are also smaller plants and grasses present on the test site terrain whose density varies greatly with the amount of recent

rainfall during the growing season. The rainfall (mostly in the form of thunder showers) was noticeably greater than usual during the early part of the test period, resulting in enhanced small plant coverage and growth.

The soil at the test site is primarily sand, with some amendment of organic matter from plant decay. Small mammals, reptiles, insects, and other animals recycle this plant material through various levels of the food chain. As an indirect result, much of the soil is well aerated and is permeated by burrows, scrapes, and mounds. Much of the soil is so well-aerated, in fact, that it is very soft, requiring much care in setting up and securing instrument tripods and towers.

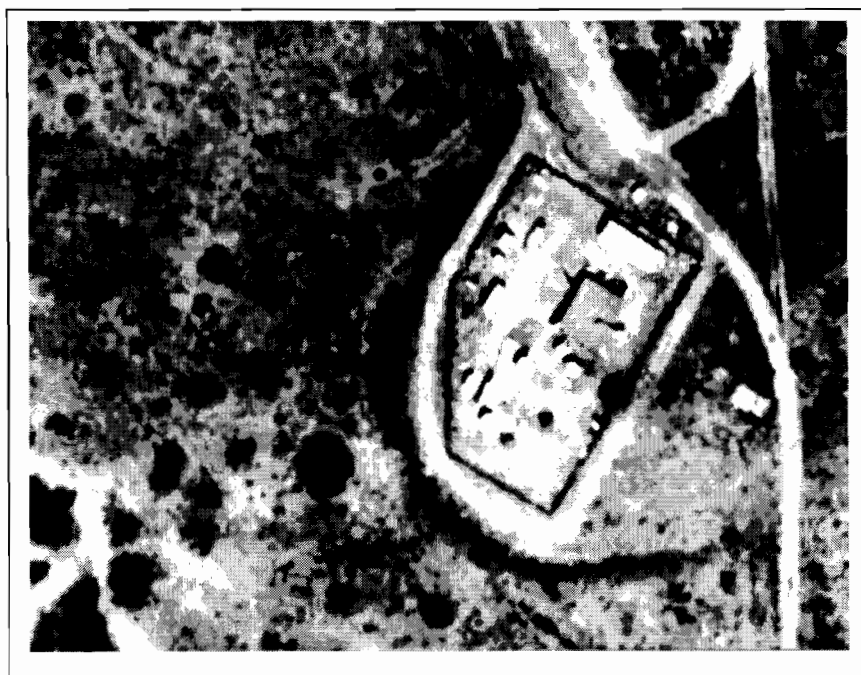


Figure 1. Aerial view of the measurement site. The compound perimeter fence is clearly seen, along with the approximate location of the horizontal measurement array (which is indicated by the red dot).

## 2) Climatological summary of test site region

We wished to conduct our measurement series over an extended period during which moisture levels were expected to range from very dry to fairly moist (relative to the norms for the desert Southwest). The dry period was expected to range from the beginning of the experiment in mid May through the end of June, with an anticipated monsoonal enhancement of the moisture levels beginning in mid July. Surface temperatures for this period are also quite warm, with highs ranging between 85° and 100° F and lows generally between 60° and 70° F. Most of the rains that occur during this period are associated with thunderstorms, which also, because of their localized nature, cause irregular patterns of wind speed and direction.

What we actually experienced as the late spring to summer seasons unfolded was a pronounced departure from the climatological average. Significant thunderstorm activity began in May and continued through the remainder of the test period reported upon here, with some multi-day respites of dry weather interspersed.

### 3) Test setup and schedule

We arranged our test series in phases to make the most of the available instrumentation and to allow our personnel time to streamline experimental procedures and work out the inevitable problems that arose. Roughly, these phases were organized into three episodes: pre-test (Phase 0) calibrations and shakedown tests of sensors; horizontal array measurements (Phases 1A and 1B) and combined horizontal array and vertical tower (Phases 2A and 2B) measurements. The analysis results provided in this report will primarily deal with the horizontal array measurement series, so that we shall only describe the Phase 1 and 2 setup geometry. Figures 2-5 depict the test layout for Phases 1A, 1B, 2A, and 2B respectively.

#### (a) Phase 1A (25 May 07 to 29 Jun 07)

This phase of the experiment was the initial operational period, though some hardware and software configuration refinements continued to be set in place. Only the horizontal array was used for this phase, with the south-to-north line of the array oriented  $330^\circ$  from north. The three Li-Cor and sonic anemometer sensor pairs were separated by 2 m and were mounted at a height of 2 m on tripods. Each Li-Cor and sonic pair had a horizontal separation distance of 20 cm, with the sonic upwind (for our initial prevailing wind direction estimate of  $240^\circ$  from north) from the Li-Cor.

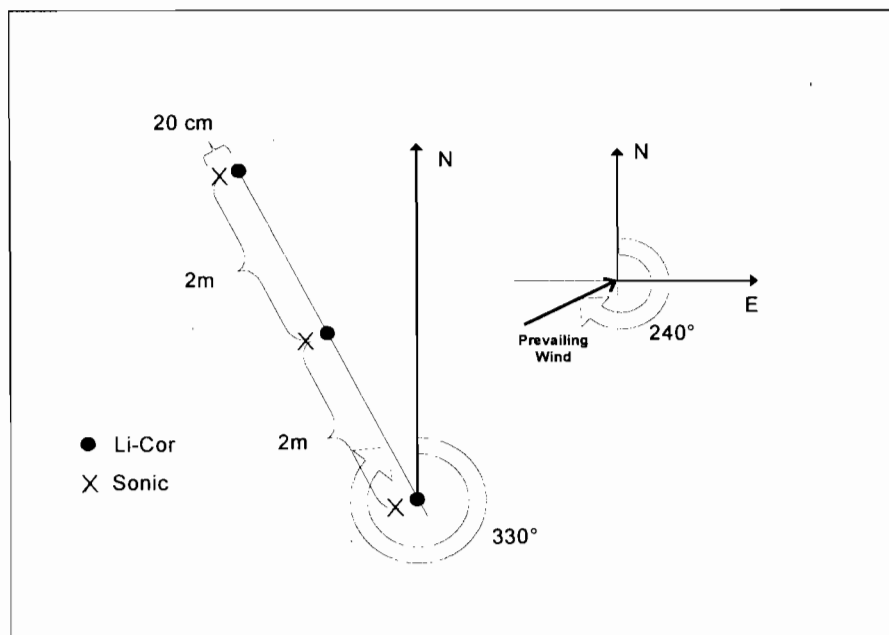


Figure 2. Phase 1A test layout for horizontal array of Li-Cor and sonic sensors.

(b) Phase 1B (29 Jun 07 to 25 Jul 07)

The measurements collected during Phase 1A indicated that the prevailing wind was more northwesterly than our initial estimate for the observing period. We therefore took the opportunity to reorient the array line to a bearing of  $20^\circ$  from north as we increased the array spacing to 4 m between sensor pairs.

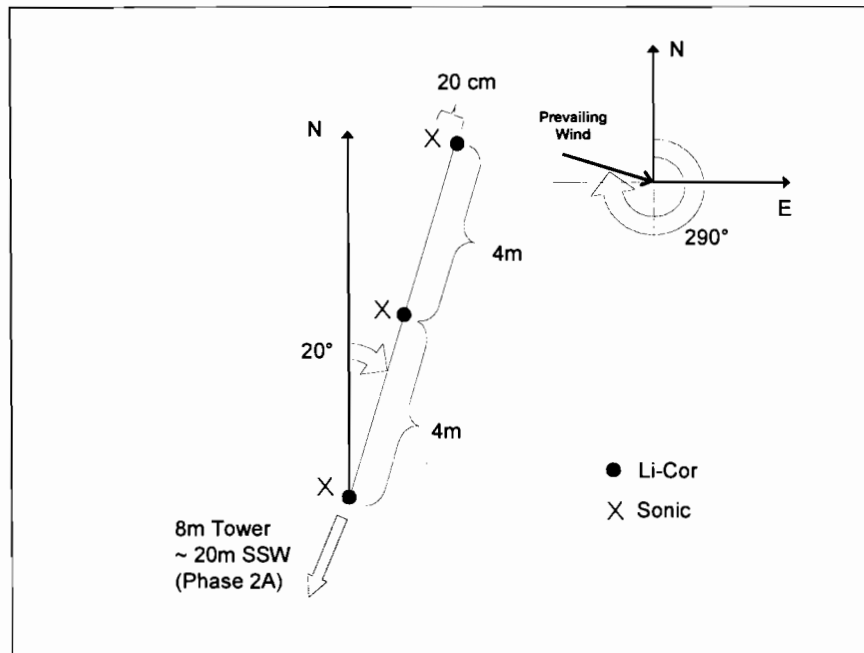


Figure 3. Phase 1B test layout for horizontal array. This layout was also used in Phase 2A.

(c) Phase 2A (25 Jul 07 to 15 Aug 07)

This phase marked the initial operation of the 8 m vertical tower array of thermistor temperature sensors and sonic anemometers, as well as the CNR1 radiometric sensor set. The tower was populated at 2, 4, 6, and 8 m above ground level with pairs of sonic and thermistor sensors. This combination was selected to provide a vertical profile of temperature and wind fluctuations, with the thermistor sensors providing a more accurate estimate of the long-term mean temperature at each level. Additional thermistor sensors were situated within 2 m of the tower at 1 m and 0.15 m (about 6 inches) above ground level. The tower was set up to be in line with the horizontal array line, at a distance of approximately 20 m from the south end of the horizontal array line. The CNR1 sensor set was situated about 4 m from the base of the tower, at a height of 2 m, on a line between the tower and the horizontal array. The horizontal array configuration was unchanged from Phase 1B for this phase of the experiment.

(d) Phase 2B (15 Aug 07 to 30 Sep 07)

The horizontal array central sensor pair was moved 2 m to the south along the existing array line for this phase, to create an asymmetric 2 m, 6 m pair spacing. This was an effort to see if more simultaneous scale information could be obtained more efficiently. The tower configuration was unchanged for this phase.

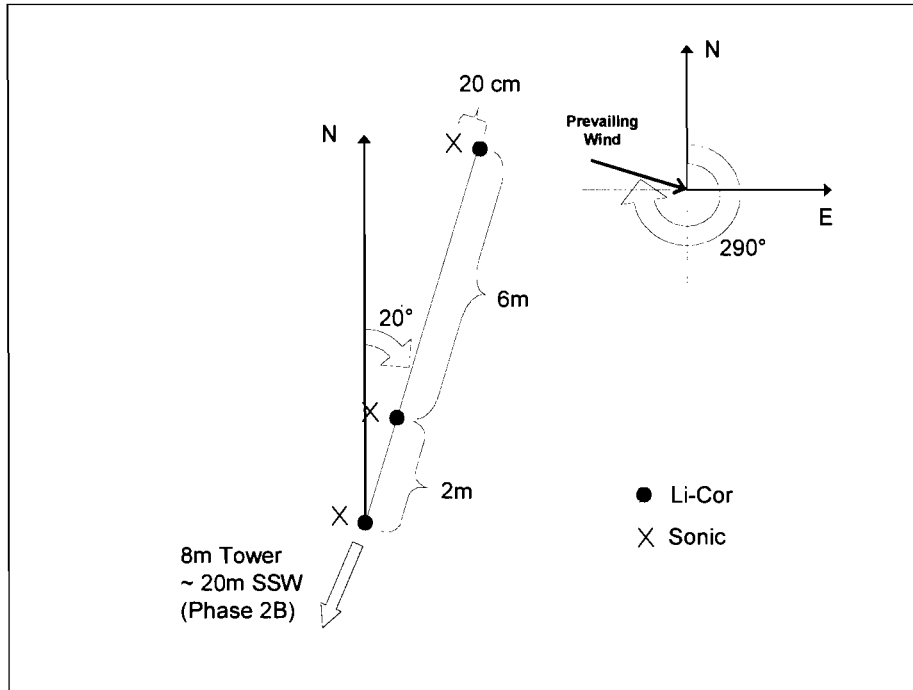


Figure 4. Horizontal array layout for Phase 2B.

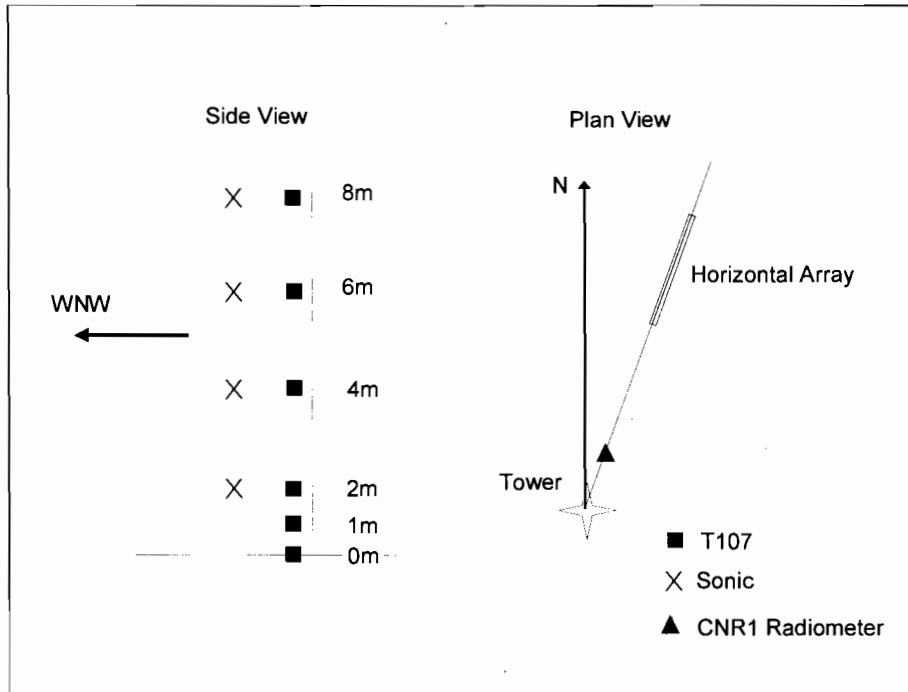


Figure 5. Tower layout for Phases 2A and 2B. Side and plan views of tower and surroundings are shown. The thermistors are labeled “T107” in this diagram.

## Data Collection and Reduction

### 1) Data collection hardware and methodology

The high speed sensors that were used in this measurement series included three Li-Cor model LI-7500 sensor systems and eight Campbell Scientific sonic anemometers. These instruments were sampled at 20 Hz to provide high resolution data for water vapor concentration, temperature, and wind component fluctuations. A lower sample rate of 1 Hz was used for the Kipp and Zonen model CNR1 sensor (for shortwave and LWIR upward/downward flux measurements) and for six thermistor-type temperature probes (which were mounted in louvered radiation shields). These last devices were used to check the accuracy of (and to normalize) the high speed temperature data measured by the sonic probes.

Three laptop computers were used to log data streams from the horizontal array and tower array sensor groupings. One laptop was located in a protective outdoor enclosure beside the tower, and archived serial (RS-232) data directly from the sonic wind sensors. This laptop also archived serial data from a Campbell CR-5000 data logger that was connected to the thermistor temperature probes and the CNR1 radiative flux sensor. A second laptop (also in a protective enclosure) located next to the horizontal sensor array archived serial data from the three Li-Cor water vapor sensors and three sonic anemometers that populated that array. The two outdoor laptops were then connected by Ethernet links to a central hub, which was located in horizontal array enclosure. A third

laptop, located in a building within the equipment compound, was used to examine and control the status of the remote computers via an Ethernet link to the hub mentioned above. These three laptop machines ran under the Fedora Core 3 or Core 6 Linux operating systems, which allowed the use of the Network File System (NFS) for mounting remote file systems, the Secure Shell (SSH) protocol for remote user login, the Secure Copy (SCP) protocol for direct copy of files from a remote system, and the Network Time Protocol (NTP) for synchronizing system clocks.

A separate laptop was also used during the test to program the CR-5000 logger so that it could serve data from sensors directly connected to it to a laptop via a serial interface. Some of the Phase 0 thermistor sensor calibration data were collected and analyzed on this computer as well.

## 2) Auditing data quality

We used various procedures to ensure that the collected data were free of pathologies, and could be used for a reasonable analysis of trends and phenomena. The sonic sensor data records ended with an error flag field that allowed for some degree of rejection of bad data. This particular automated check could be embedded in the reduction programs that we wrote in support of this effort. Another check is one that flags (what should be) fixed-length data records that are either too short or too long.

Automated techniques could not be used (at least at this point) in cases where the sensor doesn't flag questionable records or if the environment itself is causing physically incorrect sensor outputs. An instance of a rain-induced malfunction of the Li-Cor sensor readings may be seen in Figure 6, and illustrates the importance of vetting data through graphical means. This example is from the evening of 25 May 07, when a cluster of thunderstorms developed in the WSMR/Las Cruces region. The daily plot of water vapor concentration from one of the Li-Cor sensors appears normal until shortly after 2000 MDT, when the range of fluctuations suddenly widens quite markedly. This was probably caused by liquid rain water coating the windows of the transmissometer sensor. Even though we set the Li-Cor Sensors up with the recommended tilt to shed rain water, any persistent rain event will still seriously degrade accuracy until the windows are finally allowed to dry. It would perhaps be possible to provide a rain shield above the sensors, but that tactic would probably perturb the measurement results. It would also be possible that misting, wind driven rains and strong winds that frequently accompany thunderstorms could still easily erode the accuracy of the measurements or worse, damage the equipment setup.

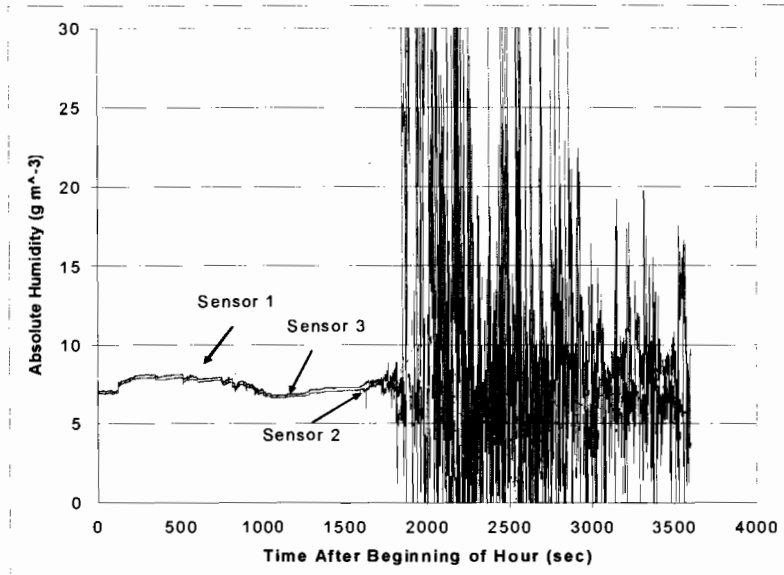


Figure 6. Li-Cor humidity sensor records for 25 May 2007, beginning at 2000 MDT. Sensors were in a horizontal linear array, with a 2 m separation (Phase 1A configuration). Sensor 1 was the northernmost, sensor 3 was the southernmost.

### 3) Daily meteorological summary

In our future data summary and analysis reports, we will include archived daily summaries of conventional meteorological parameters observed for the WSMR region. These will include the following data, which will generally be presented in graphical form:

- (a) Rawinsonde soundings for El Paso and WSMR (when available)
- (b) Air temperature
- (c) Air Pressure
- (d) Dew point
- (e) Wind speed
- (f) Wind direction
- (g) Surface weather summary (front position plots and synoptic discussion)
- (h) Precipitation radar (when rain events were seen in the area)
- (i) Satellite visible, IR, and water vapor imagery (when appropriate)

These parameters will serve to complement and check the temperature, pressure, wind component, and absolute humidity data that our high and low speed sensors collect in our test setup.

### Preliminary Data Analysis Products

#### 1) Water vapor spatial power spectra

The water vapor molar density ( $\text{mmol m}^{-3}$ ) at each sampling point was converted to an absolute humidity ( $\text{g m}^{-3}$ ) and a running mean was computed. The value of the absolute

humidity fluctuation about this running mean was then computed at each sampling point. The high speed (20 Hz sampling rate) temporal data for the UVW wind velocity components were reduced to a spatial data set by computing 1 second sliding window averages of wind speed at each data point. This, multiplied by the sampling interval time, yielded a wind run position for the given point. Because the wind speed varied from point to point, the resulting spatial one-dimensional grid of data points was non-uniformly spaced. To better accommodate the analysis of the spectrum, which uses a fast Fourier transform (FFT) that expects uniformly-spaced points, the reduction software performed an interpolation of all of the points onto a uniform grid. The grid interval simply equals the total wind run divided by (N-1), where N is the total number of fluctuation data points.

The resulting regridded absolute humidity fluctuation data were windowed with a Hanning function and then transformed via an FFT; the power spectrum was then constructed from this result. An example spectrum Li-Cor sensor 1 for 1700 – 1800 MDT on 25 May 07 is shown in Figure 7. For the most part, this spectrum follows a Kolmogorov power law behavior (a straight line of -5/3 slope for the log-log axes used here), although the spectrum drops significantly at lower spatial frequencies. Also apparent is a sharp dip in the spectrum around  $2 \times 10^{-3} \text{ m}^{-1}$ ; this is possibly due to our selection of 500 m as the exponential weighting constant for computation of the running mean. It is also evident that a point spectrum will not provide clear-cut estimates for the location of inner and outer scale humidity turbulence features. We shall therefore need to resort to cross-correlation and covariance methods to investigate departures from the inertial subrange and the structure of large scale humidity features.

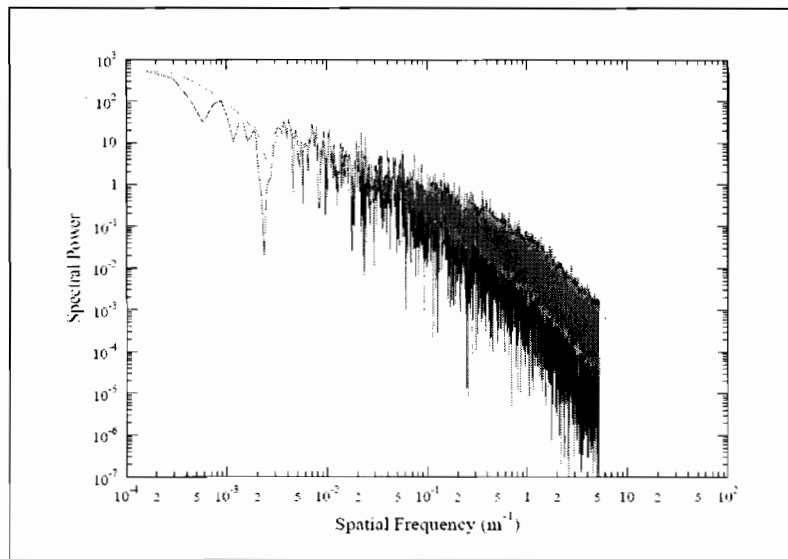


Figure 7. Example spatial power spectrum for 1700 – 1800 MDT on 25 May 07. The red curve represents the full spectrum of about 72000 points, with the green curve representing a 5-point running mean.

## 2) Cross-correlation temporal results for horizontal array

One possible way to examine the existence and strength of large scale humidity fluctuations is through the calculation of the cross-correlation function between the absolute humidity  $\rho$  measured by sensors  $i$  and  $j$ :

$$\Gamma_{\rho}(t) = \int_{-\infty}^{\infty} \rho_i(t') \rho_j(t' + t) dt' \quad (1)$$

Of course, this relation has to be numerically evaluated over the finite sampling domain, by either direct numeric means or by application of the convolution theorem for Fourier transforms. We implemented both approaches and obtained good agreement in the results. The FFT approach will be used operationally, because it is much faster, and the data sets are extensive enough to warrant its use. Figure 8 shows the 25 May 07 1500-1600 MDT results of the non-FFT calculation of cross-correlation between sensor sets 1-2, 2-3, and 1-3, which all have the same lag direction relative to the mean wind for the observing period. This consistent lag is reflected by the shift of the cross-correlation peak to negative values. The 1-3 correlation lag value (4 m baseline) is also roughly twice as large as the 1-2 or 2-3 values (2 m baseline), as expected. The maximum for the 1-3 correlation function is also lower than the 1-2 or 2-3 maxima, indicating the weaker intensity of larger humidity structures.

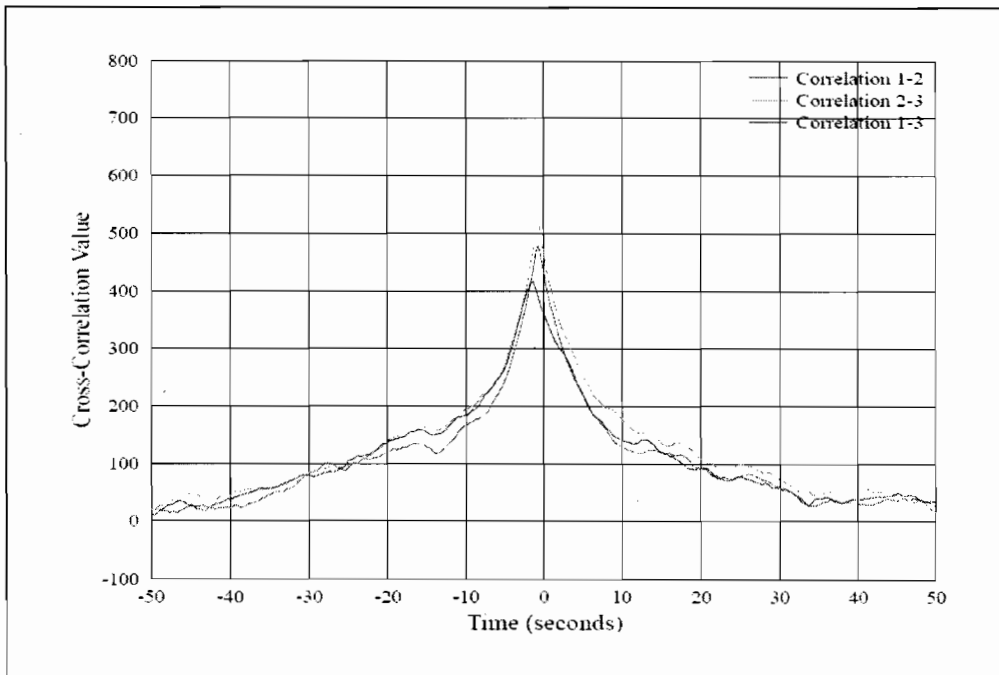


Figure 8. Example unnormalized cross-correlation for absolute humidity fluctuations for 1500 – 1600 MDT on 25 May 07.

### 3) Sensible heat flux results from tower array

The high temporal resolution wind and temperature data from the sonic sensors were reduced to yield the fluctuations

$$\begin{aligned} u' &= u(t) - \langle u \rangle_t \\ w' &= w(t) - \langle w \rangle_t \\ T' &= T(t) - \langle T \rangle_t \end{aligned} \quad (2)$$

where the brackets indicate running means at time  $t$ . The coordinate system is rotated so that the total wind vector points in the direction of  $u$  and the vertical wind component average  $\langle w \rangle_t$  is zero. With these provisos, the sensible heat flux  $H_S$  is given by the relation

$$H_S = \rho C_p \langle w' T' \rangle \quad (3)$$

and the vertical momentum flux  $\tau_m$  is given by

$$\tau_m = -\rho \langle u' w' \rangle \quad (4)$$

where  $\rho$  is the air density and  $C_p$  is the specific heat of air at constant pressure. Figure 9 shows a diurnal plot of the sensible heat flux, as derived from the tower data through relations (2) and (3) above. The general features of this plot are consistent with what we normally expect, with positive daylight values and slightly negative nocturnal values. The effect of afternoon clouds (and possibly elevated winds) can be seen in the large excursions close to sundown.

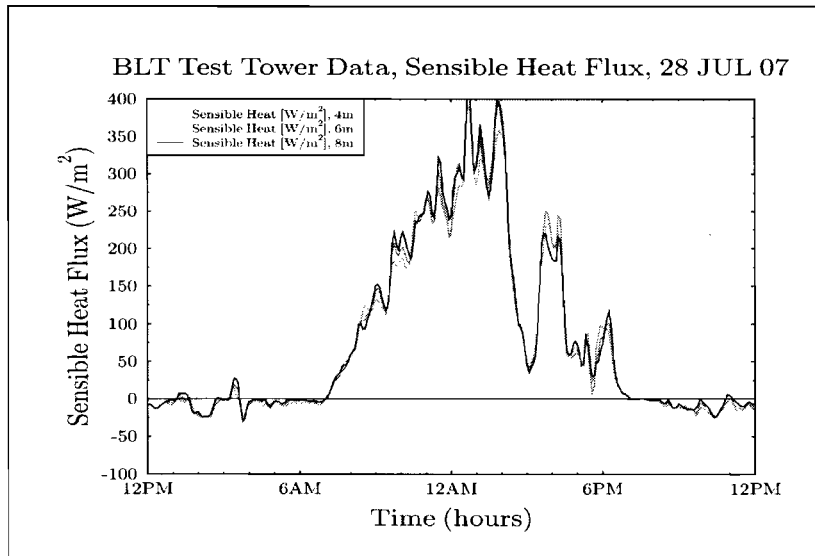


Figure 9. Diurnal plot of sensible heat flux derived from tower sonic anemometer sensor data.

Figure 10 shows a plot of the vertical momentum flux over the course of the same day as Figure 9. Again, the slightly negative values seen in the plot are normal for this quantity, but the very large negative excursion seen shortly before 6 PM local time is unusual.

This is likely due to downdraft activity from nearby thundershowers, a suspicion that is reinforced by Figure 11, which depicts the horizontal wind plot for that day. A very large spike in the horizontal wind speed occurs just before 6 PM, which probably induced a marked departure of the vertical wind component away from the local time average. The enhancement of the wind speed occurred at all tower levels, but the net positive wind speed profile gradient appears to have been maintained for most of the event. Shortly before 8 PM on this day, the wind speed fell nearly to zero, at which time the vertical temperature profile became neutral.

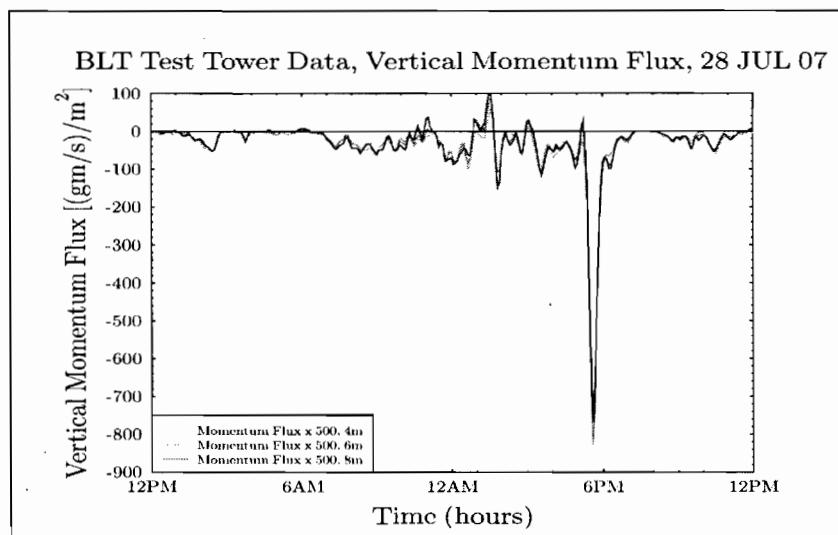


Figure 10. Diurnal plot of vertical momentum flux for the same day as the previous sensible heat flux plot.

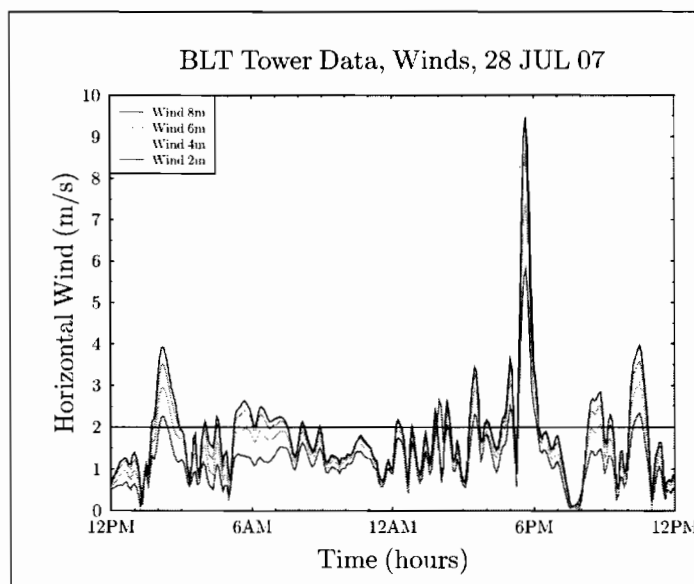


Figure 11. Plot of horizontal wind speed for the same diurnal period as the previous two plots.

#### 4) Temperature profile results from tower array

A final example of some of the tower data that were collected and analyzed is illustrated by Figure 12, which shows an hourly time series for the thermistor temperature sensors near local midnight. The plot hints at the presence of wave-like features at the 6 and 8 m tower levels, with a period of several minutes. The 1, 2, and 4 m levels only show a relatively mild variation over a much longer period.

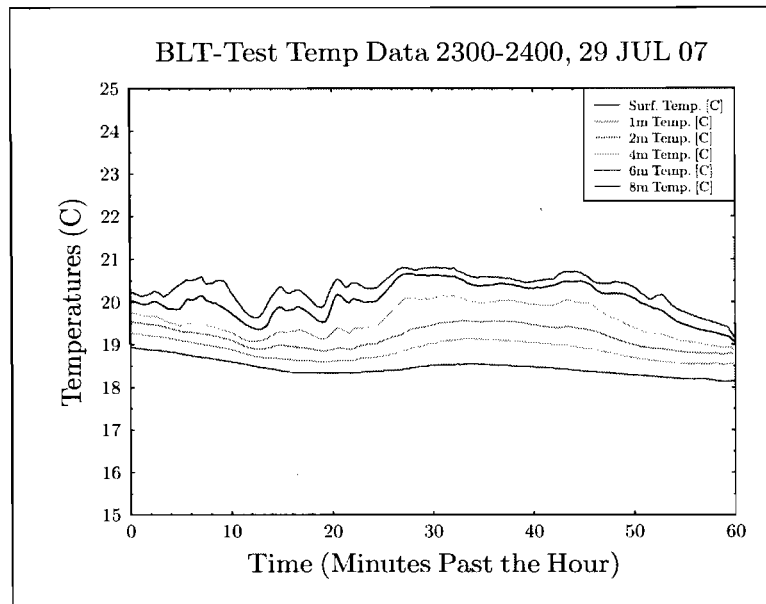


Figure 12. Tower temperature profile hourly record showing wave-like elevated disturbances

#### Conclusions and Future Plans

The first data sets from this measurement series are encouraging, as they appear to contain sufficient information to begin detailed spectral, cross correlation, and covariance analyses. The data auditing software is still being developed in response to phenomena that might complicate or invalidate results from analysis software further down the reduction chain. We will continue to refine our reduction and analysis software to capture the temporal and spatial scales that can be observed for humidity fluctuations, and compare these with what might be expected from theory.

We intend to make further use of our measurement site, which is easily secured, maintained and run on a continuous basis. The measurement data sets span large periods of time and, if the sensors are merely left to collect data without interruption, provide a very valuable climatological reference data set for a desert environment for future analysis. This is not a trivial consideration, because future deployments of terahertz or MWIR systems in this environment are fairly likely. As our analysis proceeds, phenomena will probably be identified that will merit reconfiguration of the sensor

layouts and combinations. These factors will be the subject of future discussion in a detailed analysis document, as well as open literature publications.

## **References**

Cooper, D.I., W.E. Eichinger, M. Y. Leclerc, J. Archuleta, and C. Y. J. Kao, "Coherent Microscale Surface Structures Observed by a Scanning LIDAR and their Contribution to Mass Exchange in the Stable Boundary Layer", 26<sup>th</sup> AMS Conference on Agricultural and Forest Meteorology, August 2004.

O'Brien, Sean and David Tofsted, "Development of a Terahertz Short Range Imaging Model", Proceedings of the SPIE Defense and Security Symposium, April, 2006.

O'Brien, Sean and David Tofsted, "Modeling of Atmospheric Effects on Terahertz Imaging Systems", ITEA Modeling and Simulation Conference, December 2006.

Tofsted, David, David Quintis, Sean O'Brien, Jimmy Yarbrough, Manuel Bustillos, and Gail Tirrell Vaucher, "Test Report on the November 2005 NATO RTG-40 Active Imager Land Field Trials", ARL Technical Report ARL-TR-4010, December 2006.